Applied Mathematical Modelling 82 (2020) 72–90

Contents lists available at ScienceDirect

Applied Mathematical Modelling

journal homepage: www.elsevier.com/locate/apm

Mixed convection heat transfer by nanofluids in a cavity with two oscillating flexible fins: A fluid–structure interaction approach

Esmail Jamesahar[a], Mahmoud Sabour[b], Mohammad Shahabadi[c], S.A.M. Mehryan[d], Mohammad Ghalambaz[e,f,*]

[a] Department of Mechanical Engineering, Dezful Branch, Islamic Azad University, Dezful, Iran
[b] Young Researchers and Elite Club, Ahvaz Branch, Islamic Azad University, Ahvaz, Iran
[c] Department of Mechanical Engineering, Isfahan University of Technology, Isfahan, Iran
[d] Young Researchers and Elite Club, Yasooj Branch, Islamic Azad University, Yasooj, Iran
[e] Department for Management of Science and Technology Development, Ton Duc Thang University, Ho Chi Minh City, Vietnam
[f] Faculty of Applied Sciences, Ton Duc Thang University, Ho Chi Minh City, Vietnam

ARTICLE INFO

Article history:
Received 7 September 2019
Revised 27 November 2019
Accepted 17 December 2019
Available online 20 December 2019

Keywords:
Arbitrary Lagrangian–Eulerian (ALE)
Fluid–structure interaction (FSI)
Oscillating flexible fin
Unsteady mixed convection

ABSTRACT

This study investigated the effects of two oscillating fins on the heat transfer rate and flow characteristics of a nanofluid inside a square enclosure. Both fins were attached to the hot wall and both fins oscillated at the same frequencies and amplitudes. The finite element method implemented in the arbitrary Lagrangian–Eulerian (ALE) technique was used to solve the equations describing the interactions and movements of the nanofluid and fins. Comparisons of our results and those reported in previous studies demonstrated that the modeling and numerical investigations were valid and reliable. The results showed that the increase in the heat transfer rate was due to the oscillation of the fins. In addition, the increasing trend in the heat transfer rate due to the oscillating fins decreased as the ratio of the thermal conductivity of the fins relative to the nanofluid increased. Increasing the thermal conductivity and viscosity parameters enhanced and weakened the heat transfer rate, respectively.

1. Introduction

The application of convective heat transfer has been developed in various industrial fields, and its importance has been noted recently by researchers. Mixed convection flows are combinations of free and forced convection flows, and they occur in many technological and industrial applications as well as in nature, e.g., solar receivers exposed to wind currents, electronic devices cooled by fans, heat exchangers placed in a low-velocity environment, and flows in the ocean and atmosphere [1].

Numerous studies have investigated mixed convective heat transfer. In particular, Iwatsu et al. [2] numerically investigated two-dimensional convective heat transfer based on a vertical temperature gradient, where they determined the thermofluid characteristics of fluids inside a cavity for different Richardson numbers. Oztop and Dagtekin [3] performed nu-

* Corresponding author at: Ton Duc Thang University, Ho Chi Minh City, Vietnam.
E-mail address: mohammad.ghalambaz@tdtu.edu.vn (M. Ghalambaz).

https://doi.org/10.1016/j.apm.2019.12.018
0307-904X/

merical studies of two-dimensional mixed convection in a differentially heated square cavity. The left and right walls were moving and considered at different constant temperatures. Their results showed that the Richardson number and direction of the moving walls simultaneously affected the thermofluid characteristics inside the cavity. Lamarti et al. [4] performed numerical investigations based on the lattice Boltzmann method to study the mixed convection heat transfer inside a square cavity driven by a periodically oscillating lid. They found that the Reynolds and Grashof numbers affected the energy transfer process. Radhakrishnan et al. [5] performed numerical and experimental studies of mixed convection based on a heat generating element within a ventilated cavity. They determined correlations between the average Nusselt number and the maximum dimensionless temperature within a heat source. The heat transfer performance was boosted by changing the position of the heat source. They compared their numerical results with experimental tests and they were in good agreement.

The mixed laminar convection inside a square cavity was investigated by Houat and Bouayed [6] using the lattice Boltzmann method. The results obtained for a Richardson number $Ri = 10$ were in good agreement with those produced with the finite volume method. Alsabery et al. [7] studied transient entropy generation and mixed convection for a rotating hot inner cylinder within a square cavity. They conducted numerical studies by utilizing the finite element method and arbitrary Lagrangian–Eulerian (ALE) method. The results showed that the maximum average heat transfer and global entropy generation occurred under counter-clockwise rotation of the cylinder. The ALE approach has also been utilized in other areas of physics [8].

Nanofluids have been engineered with enhanced thermal conductivity in order to augment the heat transfer in conventional fluids. Nanofluids comprise stable suspensions of nanoparticles with diameters lower than 100 nm that are dispersed well in a liquid, and the first was introduced by Choi and Eastman [9] to enhance the thermal conductivity of a fluid. Nanofluids have been proposed as new passive heat transfer enhancement techniques. Major advantages of adding nanoparticles to the host fluid are improved thermal conductivity and heat transfer. However, nanoparticles also have many other functions, such as direct solar absorption [10], fuel nano-additives [11], and antibacterial applications [12]. The present study only considered the heat transfer advantages of nanoparticles.

Mirmasoumi and Behzadmehr [13] examined the effects of the mean diameter of Al_2O_3 nanoparticles on mixed convection heat transfer within a horizontal tube. Their numerical investigations were conducted based on two-phase mixture models and the results showed that reducing the mean diameter of the nanoparticles led to increased heat transfer. Sarkar et al. [14] numerically studied the mixed convective flow and heat transfer characteristics of water–Cu nanofluids in a cross-flow along a circular cylinder. The nanoparticle volume fractions of $0 < \varphi < 25\%$ and the Reynolds number range of $0 < Re < 180$ were considered in simulations. Correlations were determined for the Nusselt number based on φ and Re. They found that the presence of nanoparticles provided a balancing force against the buoyancy force, which helped to stabilize the flow.

Aghanajafi et al. [15] numerically studied the thermal characteristics of a water–CuO nanofluid with three different volume fractions inside a triangular channel. A single-phase flow was considered for the fluid in their investigations. Considerable heat transfer enhancement was obtained using the nanofluid. In addition, the CuO nanoparticles increased the pressure loss along the channel. Nanoparticles with two different diameters did not affect the heat transfer rate.

Selimefendigil and Oztop [16] performed numerical investigations by using the finite element method to analyze mixed convection for various types of nanofluids (water/Cu, Al_2O_3, and TiO_2) in a three-dimensional cavity with two inner adiabatic circular cylinders. They found that water–Cu had the highest heat transfer rate. The direction of rotation for the cylinders led to either an increase or decrease in the Nusselt number. They also determined correlations with the Nusselt number based on the Rayleigh number and angular rotational speed of the cylinders. Kareem and Gao [17] numerically studied mixed convection heat transfer for four different types of fluids (nanoparticles with different diameters) inside an enclosure. Their simulations were conducted under three-dimensional unsteady flow conditions with a two-phase mixture model. The results showed that utilizing a nanofluid instead of a conventional fluid considerably affected the heat transfer and flow pattern. The size and volume fraction of the nanoparticles significantly influenced the heat transfer. Previous reviews have also discussed the enhancement of convective heat transfer by using nanofluids and inside enclosures [18–20]. Nanofluids have been applied to improve the design of radiators [21], reduce entropy generation [22], and improve the heat transfer in boundary layers [23]. Studies have also investigated the thermal properties of nanofluids [24] as well as simulating liquid flows and heat transfer in nano-passages [25–28].

As mentioned above, the force factor for mixed convection in an enclosure can be the motion of a wall of the enclosure, i.e., lid driven [29,30]. In addition to the movements of the boundaries of cavities and membranes, the oscillation of a fin attached to a wall can disturb the fluid and induce a mixed convection flow. For instance, the effects of fluid–structure interactions (FSI) on mixed convection within a cavity where a flexible elastic fin was attached to the bottom wall were investigated by Ismael and Jasim [31], who found that a flexible fin increased the Nusselt number more than a rigid fin.

Various characteristics of heat transfer have been investigated in the presence of rigid fins, such as the fin inclination angle [32,33] and length [34], as well as the presence of fins on the internal parts of a cavity [35], fins in a mixed convection flow [36], and an array of fins subject to mixed convection [37,38]. Many studies have focused on the thermal effects of attached fins on heat transfer in a cavity, but few have investigated the effects of the presence of a flexible fin on heat transfer.

FSI involves a deformable structure as well as the flow field and heat transfer. In general, it is considered that the finite element method is suitable for handling the structure, and the finite volume method for dealing with the fluid and temperature field. However, in many new numerical schemes, the behavior of the solid structure can be handled using the finite

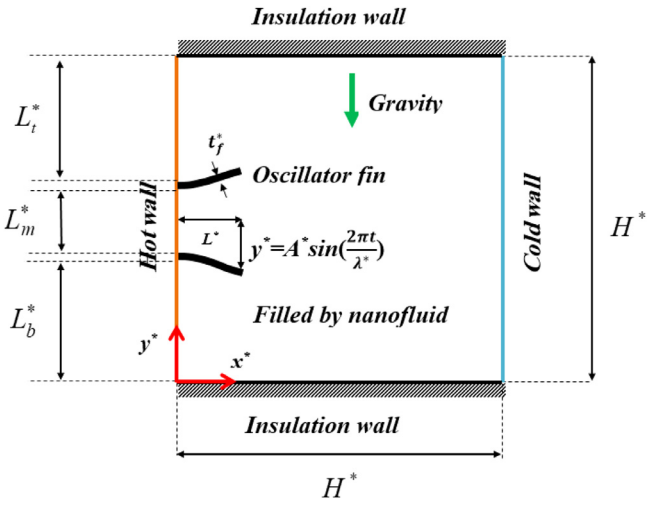

Fig. 1. Schematic representation of the cavity with two oscillating fins.

volume method. For example, Barton et al. [39] investigated the large deformation of solid structures using an Eulerian finite volume scheme. Moreover, the fluid and temperature fields can be solved with the finite element method [40–42]. Hence, recently developed numerical schemes can be employed for handling FSI problems using a finite element method or finite volume method. In particular, PHOENICS codes can be utilized to solve an FSI problem with the finite volume method [43]. Many excellent books [44] and other publications [45,46] have described the solution of FSI problems using the finite element method. The finite element method was employed to handle the evolving FSI model in the present study.

Considering the finite element method, Ghalambaz et al. [47] numerically studied the FSI for an oscillating fin attached to the hot wall of a cavity. Both the buoyancy forces and excitation were considered for the fin. The results showed that increasing the amplitude of the oscillating fin enhanced the Nusselt number. The optimized non-dimensional length for obtaining better heat transfer and greater compatibility with the oscillating amplitudes was 20% of the size of the cavity. Selimefendigil et al. [48] numerically studied the thermofluid characteristics of a Cu–water nanofluid in a vertical lid-driven square cavity with a flexible fin attached to the upper wall. The cavity was subject to an inclined magnetic field. The effects of the fin elasticity on the thermofluid characteristics of the cavity were explored. The results showed that the heat transfer was better when the fin was more flexible (lower Young's modulus).

Based on flexible fins in cavities and using the finite element method, Raisi and Arvin [49] explored the effect of the presence of a flexible baffle at the center of a cavity, while Zadeh et al. [50] investigated the effect of the location of a flexible baffle in a cavity. The results showed that a flexible baffle could improve the heat transfer. Alsabery et al. [51] theoretically investigated the effect of an oscillating fin on the bottom wall of an oblique cavity and showed that increasing the fin oscillation amplitude enhanced the heat transfer.

Previous reviews of oscillating flexible fins [47–51] have analyzed the effect of the presence of a single flexible fin or baffle. However, the presence of two active flexible fins can considerably change the flow behavior in a cavity by inducing pumping effects on the fluid trapped between the fins. This effect has not been investigated comprehensively in previous studies. Hence, the present study investigated the effects of two oscillating flexible fins on the mixed convection flow and heat transfer in an enclosure. Moreover, this is the first study to consider the effects of flexible oscillating fin and nanofluids.

2. Problem description

2.1. Physical model

Fig. 1 illustrates the geometry and physical model of a square cavity with size H^* and two flexible oscillating fins. It is assumed that the length of the Z-direction dimension of the cavity is much greater than that those of the two horizontal and vertical dimensions, so the assumption of a two-dimensional cavity can be considered in numerical investigations. The temperatures of the left and right walls are constant, and they are assumed to be the higher and lower temperatures T_h and T_c, respectively. In addition, both of the horizontal walls are considered to be well insulated. Two flexible thin fins are mounted on the left hot vertical wall. The fins are aligned symmetrically with respect to the mid-height of the cavity ($H^*/2$) and the distance between fins is $H^*/5$. The fins oscillate at a specified amplitude and frequency. It should be noted that the fins start to oscillate when the natural convection reaches a steady state. The working fluid comprises nanoparticles with a volume fraction of C, which are dispersed well in a Newtonian and incompressible base fluid. Furthermore, Boussinesq's approximation is considered for modeling the buoyancy forces. It is also assumed that the flow is laminar, and thus the turbulence effects are neglected.

2.2. Basic equations

The governing equations based on the FSI principles and ALE for the geometrically nonlinear elastodynamic structural displacement and energy of the flexible fins are defined as [47,52]:

$$\rho_s \frac{d^2 d_s^*}{dt^2} - \nabla^* \sigma^* = F_v^* \tag{1}$$

$$(\rho C_p)_s \frac{\partial T}{\partial t} = k_s \nabla^{*^2} T, \tag{2}$$

where σ^* represents the stress tensor, d_s^* is the vector of solid displacement, and F_v^* is the body force, including the weight of the flexible fin and the buoyancy force in the fluid. The basic conservation equations for the continuity, momentum, and energy in the ALE formulation are defined as [47,53]:

$$\nabla^* \cdot u^* = 0 \tag{3}$$

$$\frac{\partial u^*}{\partial t} + (u^* - w^*) \cdot \nabla^* u^* = -\frac{1}{\rho_{nf}} \nabla^* P^* + \nu_{nf} \nabla^{*^2} u^* + \beta_{nf} g_y (T - T_c) \tag{4}$$

$$(\rho C_p)_{nf} \left(\frac{\partial T}{\partial t} + (u^* - w^*) \cdot \nabla^* T \right) = k_{nf} \nabla^{*^2} T, \tag{5}$$

where u^* represents the nanofluid velocity vector, w^* is the velocity of the moving mesh, P^* denotes the pressure field inside the nanofluid, T denotes the temperature field, ρ_s and ρ_{nf} are the density of the solid and nanofluid, respectively, β_{nf} and ν_{nf} are the volumetric thermal expansion coefficient and kinematic viscosity of the nanofluid, and g_y is the acceleration due to gravity. The streamlines can be obtained by defining the following stream function ψ^*.

$$\nabla^{*^2} \psi^* = -\nabla^* \times u^* \tag{6}$$

Assuming that the flexible fin is linear elastic and considering nonlinear geometry effects, the stress tensor is defined as [47]:

$$\sigma = J^{-1} F S F^{tr}, \tag{7}$$

where $F = (I + \nabla^* d_s^*)$ and $J = det(F)$. The second Piola–Kirchhoff stress tensor (S) and strain (ε) are related to each other as:

$$S = C : (\varepsilon), \varepsilon = \frac{1}{2} \left(\nabla^* d_s^* + \nabla^* d_s^{*^{tr}} + \nabla^* d_s^{*^{tr}} \nabla^* d_s^* \right), \tag{8}$$

where $C = C(E, \nu)$. The initial and boundary dimensional conditions can be written as follows.

$$u^*(x^*, y^*, 0) = 0, w^*(x^*, y^*, 0) = 0, T(x^*, y^*, 0) = T_p = \frac{T_h + T_c}{2} \tag{9-a}$$

$$u^*(0, y^*, t) = u^*(H^*, y^*, t) = 0 \tag{9-b}$$

$$u^*(x^*, 0, t) = u^*(x^*, H^*, t) = 0 \tag{9-c}$$

$$T(0, y^*, t) = T_h, T(H^*, y^*, t) = T_c, \left. \frac{\partial T}{\partial y^*} \right|_{(x^*, 0, t)} = \left. \frac{\partial T}{\partial y^*} \right|_{(x^*, H^*, t)} = 0 \tag{9-d}$$

As mentioned above, the fins start to oscillate due to an external vibration when the natural convection reaches a steady state. The external displacement of the top part of the fins is defined as follows.

$$y^* = A^* \sin \left(\frac{2\pi t}{\lambda^*} \right) \tag{10}$$

The displacement is zero at initial times and starts when the flow reaches to about a steady-stated condition. The no-slip boundary condition is considered for the walls. The walls of the cavity are also impermeable. The continuity of the kinematic forces and dynamic movements are the boundary conditions for the FSI at the fins, which yield the following.

$$\frac{\partial d_s^*}{\partial t} = u^*, \sigma^* \cdot n = \left[-P^* I + \mu_{nf} \nabla u^* \right] \cdot n \tag{11}$$

Moreover, the energy balance at the solid–fluid interface can be written as:

$$k_{nf} \left. \frac{\partial T}{\partial n} \right|_{nf} = k_s \left. \frac{\partial T}{\partial n} \right|_s. \tag{12}$$

The non-dimensional parameters are introduced as follows.

$$d_s = \frac{d_s^*}{H^*}, \sigma = \frac{\sigma^*}{E}, \tau = \frac{t\alpha_{bf}}{H^{*2}}, (x, y) = \frac{(x^*, y^*)}{H^*}, \lambda = \frac{2\pi H^{*2}}{\lambda^* \alpha_{bf}}, \theta = \frac{T - T_c}{T_h - T_c}$$
$$\left(A, L, t_f, L_b, L_m, L_t\right) = \frac{\left(A^*, L^*, t_f^*, L_b^*, L_m^*, L_t^*\right)}{H^*}, (u, w) = \frac{(u^*, w^*)H^*}{\alpha_{bf}}, P = \frac{H^{*2}}{\rho_{bf}\alpha_{bf}^2}P^* \tag{13}$$

The governing equations for Eqs. (1)–(6) are rewritten in non-dimensional form as:

$$\frac{1}{\rho_R}\frac{d^2 d_s}{d\tau^2} - E_\tau \nabla\sigma = E_\tau F_v \tag{14}$$

$$\frac{(\rho C_p)_s}{(\rho C_p)_{bf}}\frac{\partial\theta}{\partial\tau} = \kappa\nabla^2\theta \tag{15}$$

$$\frac{\partial u}{\partial t} + (u - w)\cdot\nabla u = -\frac{\rho_{bf}}{\rho_{nf}}\nabla P + \frac{\rho_{bf}}{\rho_{nf}}\frac{\mu_{nf}}{\mu_{bf}}Pr\nabla^2 u + \frac{\beta_{nf}}{\beta_{bf}}RaPr\theta \tag{16}$$

$$\frac{(\rho C_p)_{nf}}{(\rho C_p)_{bf}}\left(\frac{\partial\theta}{\partial\tau} + (u - w)\cdot\nabla\theta\right) = \frac{k_{nf}}{k_{bf}}\nabla^2\theta \tag{17}$$

$$\nabla^2\psi = -\nabla\times u, \tag{18}$$

where

$$Ra = \frac{g_y\beta_{bf}(T_h - T_c)H^{*3}}{\upsilon_{bf}\alpha_{bf}}, Pr = \frac{\upsilon_{bf}}{\alpha_{bf}}, E_\tau = \frac{EH^{*2}}{\rho_f\alpha_f^2}$$
$$F_v = \frac{\left(\rho_{nf} - \rho_s\right)H^* g_y}{E}, \rho_R = \frac{\rho_{nf}}{\rho_s}, \kappa = \frac{k_s}{k_{bf}} \tag{19}$$

In the equations above, Ra is the Rayleigh number, Pr is the Prandtl number, E_τ represents the non-dimensional flexibility, F_v indicates the parameter of the body force, and ρ_R denotes the parameter of the density ratio. It should be noted that when the fluid is heavier than the fin, F_v has a positive value. The non-dimensional forms of the initial and boundary conditions for Eqs (9-a) to (9-d) are also provided as follows.

$$u(x, y, 0) = w(x, y, 0) = 0, \theta(x, y, 0) = \theta_p = 0.5 \tag{20-a}$$

$$u(0, y, \tau) = u(1, y, \tau) = 0 \tag{20-b}$$

$$u(x, 0, \tau) = u(x, 1, \tau) = 0 \tag{20-c}$$

$$\theta(0, y, \tau) = 1, \theta(1, y, \tau) = 0, \left.\frac{\partial\theta}{\partial y}\right|_{(x,0,\tau)} = \left.\frac{\partial\theta}{\partial y}\right|_{(x,1,\tau)} = 0 \tag{20-d}$$

The non-dimensional solid–fluid interaction and energy balance boundary conditions can be written as:

$$\frac{\partial d_s}{\partial\tau} = u, E_\tau\sigma\cdot n = \left[-PI + \frac{\mu_{nf}}{\mu_{bf}}Pr\nabla u\right]\cdot n \tag{21}$$

$$\left.\frac{\partial\theta}{\partial n}\right|_{nf} = \kappa\left.\frac{\partial\theta}{\partial n}\right|_s. \tag{22}$$

It should be noted that the fin oscillation in a non-dimensional form can be represented by $y = A\sin(\lambda.\tau)$ when $\tau > 0.5$. The displacement is zero when $\tau < 0.5$. In the present study, it is assumed that the only important parameters for the nanofluid are the dynamic viscosity and thermal conductivity. Hence, in order to further generalize the study, the density ratio and thermal expansion ratio are treated as unity [54].

$$\frac{k_{nf}}{k_{bf}} = 1 + NcC \tag{23-a}$$

$$\frac{\mu_{nf}}{\mu_{bf}} = 1 + N\nu C \tag{23-b}$$

Table 1
Grid study using $Ra = 10^5$, $Pr = 7$, $L = 0.2$, $A = 0.1$, $\lambda = 0.1$, and $\kappa = 100$.

Case number	CPU	Memory (MB)	Run time (min)	Domain elements	Boundary elements
1	4	1000	31	5625	395
2	4	1150	46	8719	543
3	4	1300	52	11882	694
4	**4**	**1400**	**71**	**14987**	**845**
5	4	1500	86	16957	943

2.3. Heat transfer rate

In this study, the Nusselt number is the parameter of interest, where it represents the heat transfer from the hot wall. The local Nusselt number for the left hot wall is defined as:

$$Nu = \frac{hH^*}{k_{bf}}, \tag{24}$$

where h is the convective heat transfer coefficient at the left wall. Using the energy balance at the hot left wall gives:

$$h(T_h - T_c) = -k_{nf}\partial T/\partial x^* \tag{25}$$

where invoking the non-dimensional parameters yields:

$$Nu_{nf} = -\frac{k_{nf}}{k_{bf}}\frac{\partial \theta}{\partial x}. \tag{26}$$

In addition, considering the energy balance at the interface of the left wall and the fin as well as the non-dimensional parameters gives the following.

$$Nu_s = -\kappa\frac{\partial \theta}{\partial x} \tag{27}$$

Hence, the average Nusselt number on the hot wall is defined as follows.

$$Nu_t = \int_0^{s_1} Nu_{nf}dy + \int_{s_1}^{s_2} Nu_s dy + \int_{s_2}^{s_3} Nu_{nf}dy + \int_{s_3}^{s_4} Nu_s dy + \int_{s_4}^{H} Nu_{nf}dy$$

$$\begin{cases} s_1 = \dfrac{H}{2} - \dfrac{3t_f}{2} - 0.1\ , \quad s_2 = \dfrac{H}{2} - \dfrac{t_f}{2} - 0.1 \\ s_3 = \dfrac{H}{2} + \dfrac{t_f}{2} + 0.1\ , \quad s_4 = \dfrac{H}{2} + \dfrac{3t_f}{2} + 0.1 \end{cases} \tag{28}$$

3. Numerical method and validation

3.1. Numerical method and grid examination

Using a numerical method to solve the nonlinear and coupled dimensionless equations presented as Eqs. (13)–(17) together with the imposed initial and boundary conditions defined by Eqs. (20)–(22) is unavoidable. Hence, the Galerkin finite element method and the ALE technique were implemented to solve the weak forms of the equations. The numerical approach was explained in detail in a previous study [55]. Fig. 2 shows the algorithm utilized to solve the equations. In a numerical study, examining the grid independence is one of the most important steps for ensuring the accuracy of the computations. Hence, grid independence analysis was conducted to ensure that the results were independent of the number of grid elements. As shown in Fig. 3, triangular non-structured elements and boundary-shape elements were employed to discretize the fluid domain. Structured elements were used for the solid fins. It should be noted that the grid study was performed using the following non-dimensional parameters: $Ra = 10^5$, $Pr = 7$, $L = 0.2$, $\kappa = 100$, $A = 0.1$, $C = 5\%$, and $\lambda = 0.1$. According to Table 1 and Fig. 4, the difference in the transient average Nusselt numbers was negligible for cases 4 and 5, and thus case 4 with 14987 domain elements and 845 boundary elements was selected for the numerical calculations. Fig. 5 shows that the maximum velocity magnitude inside the cavity at the steady state was not affected considerably by the number of the elements, so case 4 could provide accurate and correct results. The run time was 71 min for the grid with case 4. The system used for the numerical simulations included 16 GB of memory and eight CPU cores, where each operated at 2.7 GHz.

3.2. Validation

The study described by Küttler and Wall [56] was employed to validate the FSI code. Küttler and Wall [56] studied a cavity with a flexible bottom wall and moving top wall. The top wall of the square cavity was driven at a velocity of

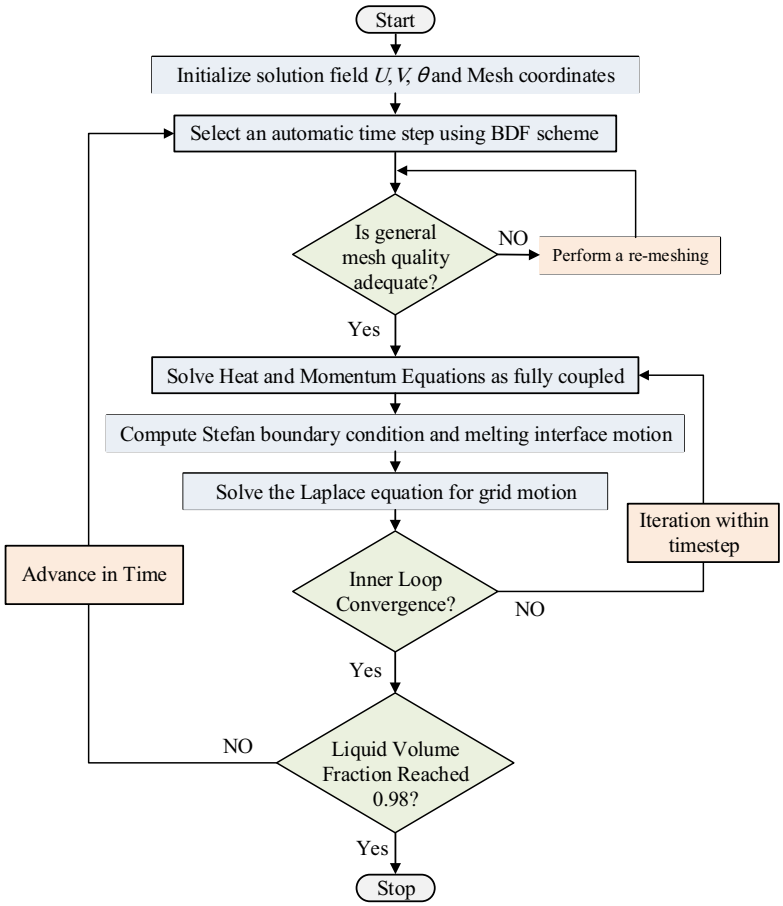

Fig. 2. Schematic illustration of the solution algorithm.

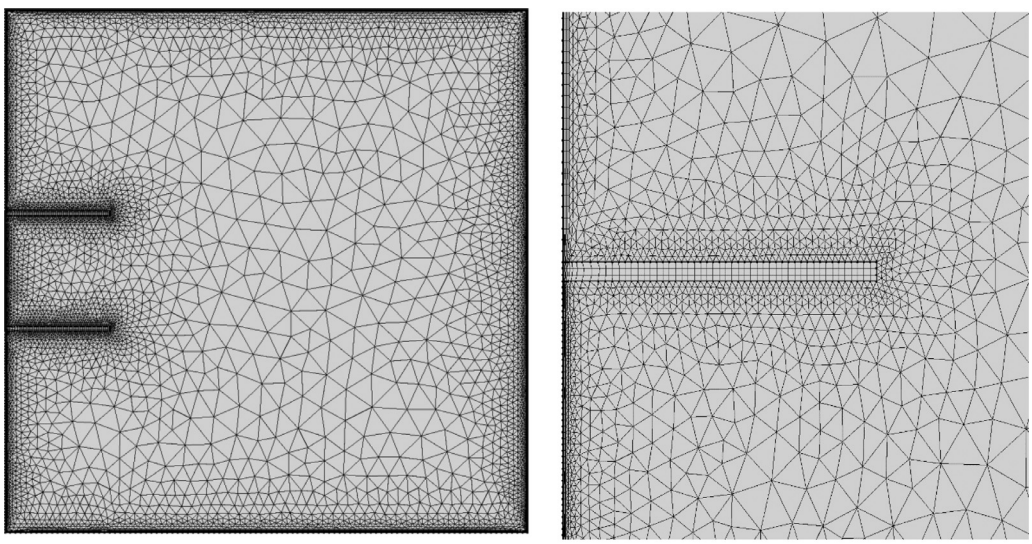

Fig. 3. Schematic showing the utilized grid (a) for the entire solution domain and (b) by focusing on the fin with a structured mesh.

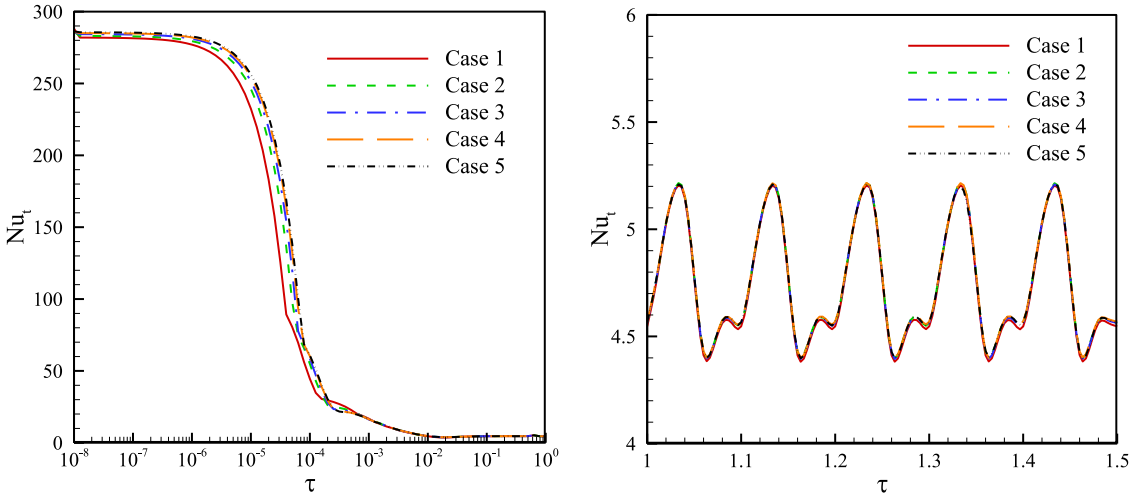

Fig. 4. Average Nusselt number versus time for different grid numbers using $Ra = 10^5$, $Pr = 7$, $L = 0.2$, $\kappa = 100$, $A = 0.1$, $C = 5\%$, and $\lambda = 0.1$

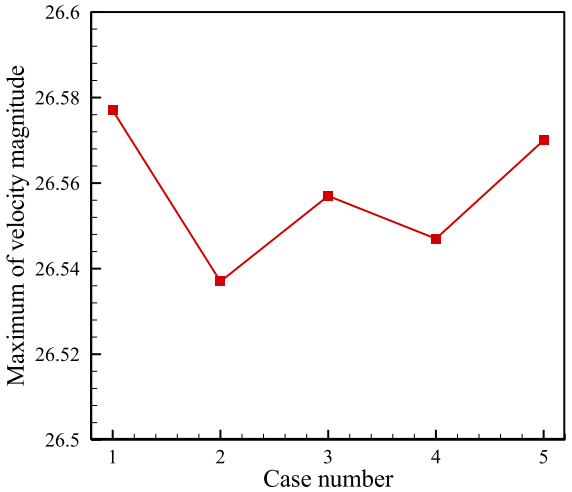

Fig. 5. Maximum velocity magnitude inside the cavity with different mesh sizes.

Table 2
Properties of the fluid and flexible wall according to Küttler and Wall [56].

Property	Fluid	Flexible wall
Kinematic viscosity (υ_f)	0.01 m^2/s	–
Density (ρ)	1 kg/m^3	500 kg/m^3
Poisson's ratio(v_s)	–	0
Young's modulus (E)	–	250 N/m^2
Thickness	–	0.002 m

$u_x = (1\text{-}\cos(2\pi t/5))$ m/s, and two free boundaries were considered above the left and right walls. Therefore, the lower wall was altered by the interaction between the fluid and solid when moving the upper wall due to its effect on the fluid inside the cavity and the creation of a vortex within. The changes in the form of the flexible wall were studied over time. Table 2 shows the properties of the fluid and the flexible wall. Fig. 6 compares the results obtained in the present study and those reported by Küttler and Wall [56] in terms of the shape of the flexible wall after $t = 7.5$ s. The comparison shows that the agreement between the results was satisfactory.

The study described by Kahveci [57] was considered in order to validate the nanofluid heat transfer in the enclosure. Kahveci [57] studied the free heat transfer in a square cavity filled with a nanofluid. The volume fraction range for the nanoparticles was also treated as between 0% and 20%. However, it should be noted that the volume fraction of nanoparticles was not considered to exceed 5% in the present study, and thus the high volume fractions was used for comparisons with

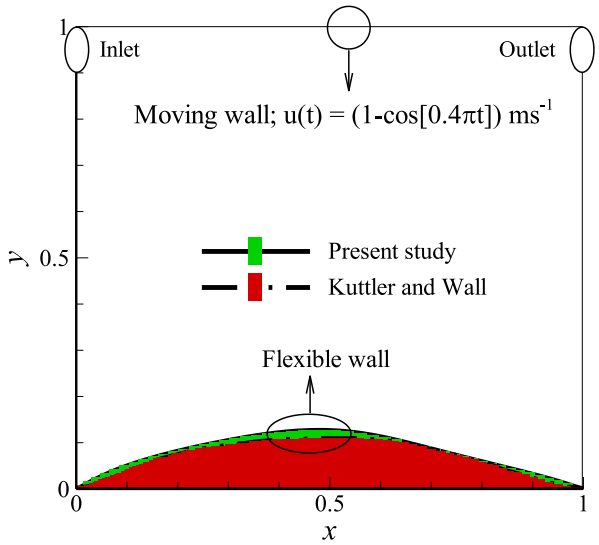

Fig. 6. Comparison of the results obtained in the present study and those reported by Küttler and Wall [56].

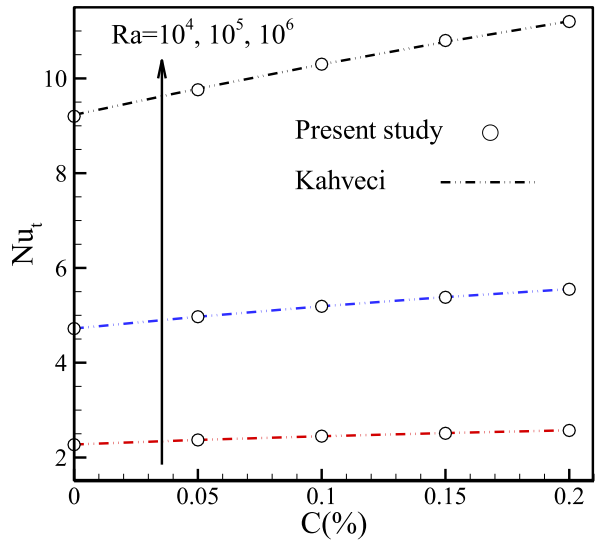

Fig. 7. Comparison of the results obtained in the present study and those reported by Kahveci [57].

the previously reported results. Fig. 7 shows that the results obtained in the present study and those reported by Kahveci [57] were in good agreement.

4. Results and discussion

The present study investigated the effects of the non-dimensional variable parameters given in Table 3 on the temperature field, velocity distribution, streamlines within the enclosure, and heat transfer rates on the hot wall. The results obtained in the present study are generally reported for the default values of the non-dimensional parameters; otherwise, the values of the non-dimensional parameters are stated.

Figs. 8 and 9 illustrate the velocity and temperature fields within the square cavity during the convection process, respectively. As shown in Fig. 8, at the initial time ($\tau = 10^{-4}$), the relative flow velocity was zero and some minor movements occurred next to the vertical walls. The velocity increased near the cold wall as well as at the upper and bottom part of the warm wall (Fig. 8(b)). At $\tau = 10^{-3}$, the flow velocity increased beside the cold wall. Subsequently, all of the small local vortexes inside the cavity disappeared and a large vortex formed at the center of the cavity. At $\tau = 10^{-2}$, the maximum flow velocity occurred next to the cold wall. The fins are allowed to oscillate at $\tau = 0.5$. The fins then started vibrating and the flow velocity reached its maximum at the tips of the oscillating fins and next to the cold wall. Fig. 9 illustrates

Table 3
Ranges of the non-dimensional parameters.

Parameter	Default value	Minimum value	Maximum value
Ra	10^5	10^4	10^6
Pr	7	–	–
K	100	1	1000
C (%)	5	0	8
Nc	8	–	–
Nv	8	4	16
λ	0.1	0.05	0.5
A	0.1	0.01	0.1

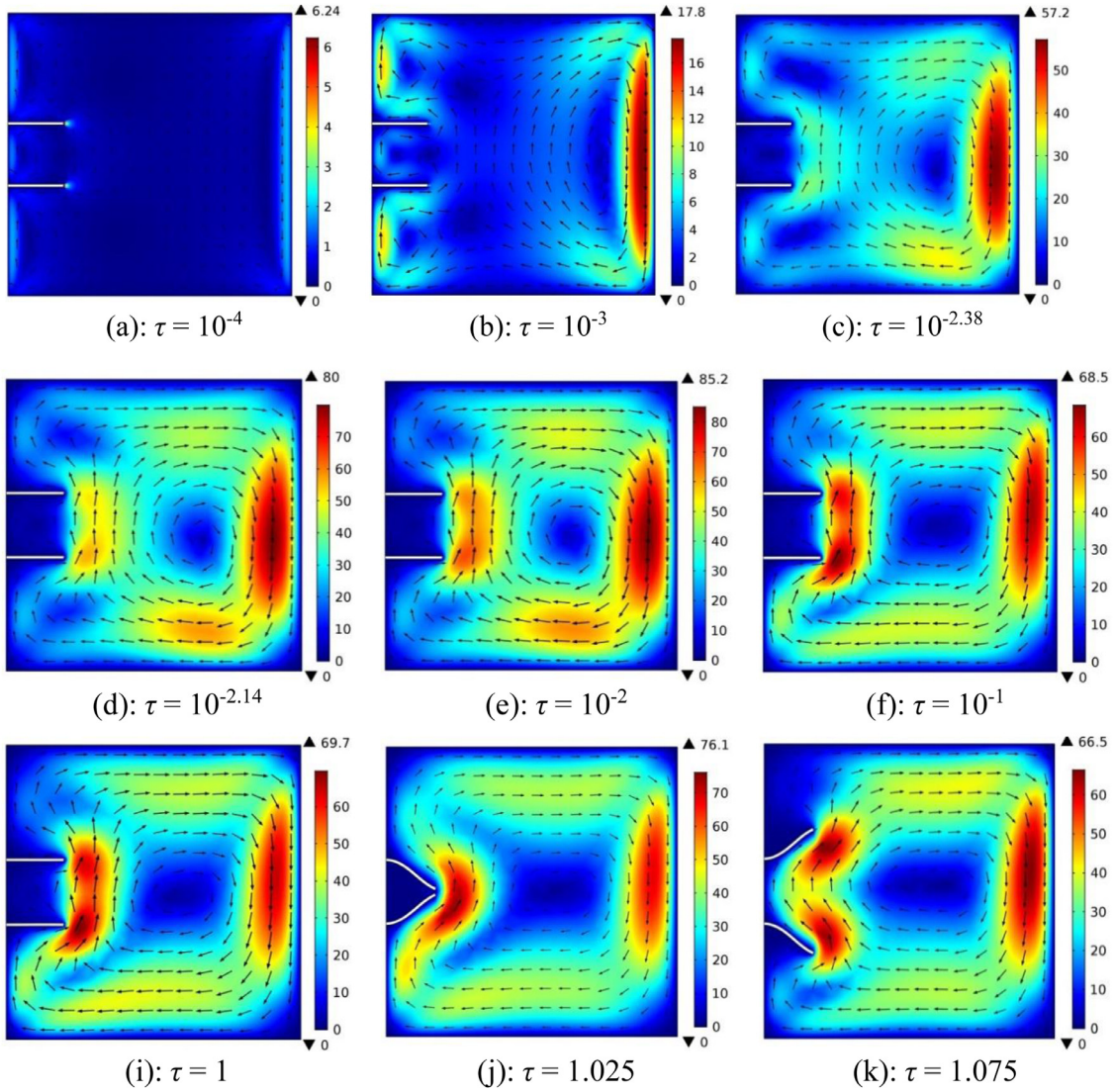

Fig. 8. Velocity contours and flow directions.

the non-dimensional temperature distributions at various times inside the cavity. As time passed, the upper and lower walls of the cavity became warmer and colder, respectively, because of the flow circulation induced inside the cavity. In the opened fins position, the temperature gradient was clearly higher than that in the closed position because of the higher flow velocity in the opened position. The wall at the upper area of the fins finally became warmer compared with the bottom area because of free convection heat transfer effects.

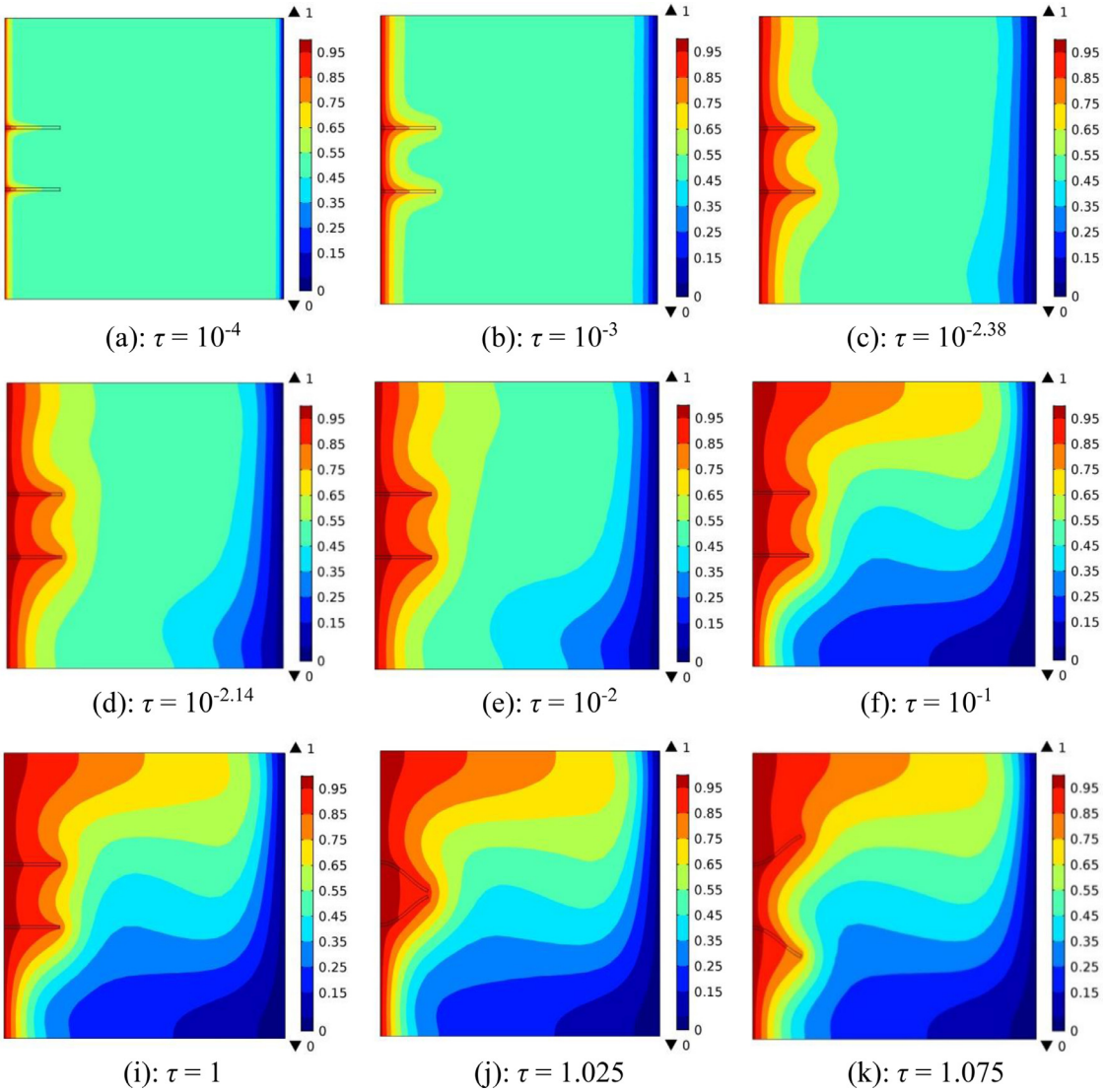

Fig. 9. Distributions of non-dimensional temperature in the cavity.

Fig. 10 illustrates the vorticity contours at different time points. The strength of the vorticity tended to increase before reaching a steady state. The strength of the vorticity next to the fins accounted for most of that within the cavity. The closed fins configuration obtained the highest vorticity strength, whereas the opened fins position resulted in the lowest. In fact, the behavior of the vorticity contours followed the velocity field depicted in Fig. 8.

Figs. 11(a) and (b) show the streamlines and isotherms inside the enclosure at various Rayleigh numbers when the fins reached the maximum amplitude. Two stagnation points were observed at the tips of the opened fins and one stagnation point for the closed fins, as shown clearly in the images of the streamlines. At low Rayleigh numbers, the streamlines indicating uniform patterns exhibited a smooth flow circulation inside the enclosure. At $Ra = 10^4$, the isotherms had a semi-vertical distribution, thereby demonstrating the dominant influence of the conduction heat transfer regime. As the Rayleigh number increased, the advection mechanism played a critical role, and thus the isotherms started to follow the flow patterns and they became horizontal at $Ra = 10^6$. At higher Rayleigh numbers, i.e., $Ra = 10^6$, the strength of the streamlines was boosted due to buoyancy effects and the density of the streamlines confirmed this change.

Figs. 12(a), (b), and (c) show the local Nusselt numbers on the bottom, middle, and top segments of the hot wall, respectively, in the last second. These figures illustrate four different states for the fins and fluid, with rigid/flexible fins and pure fluid/nanofluid. The intense heat transfer variations at the lower part of the hot wall compared with the two other parts of the wall were due to its primary contact with the cold fluid/nanofluid, which did not occur in the areas on the middle and upper walls. In general, when the cold fluid/nanofluid approached the lower part of the hot wall, the drastic differences in temperature between the wall and fluid led to high temperature gradients and heat transfer rates. Thus, the local Nusselt

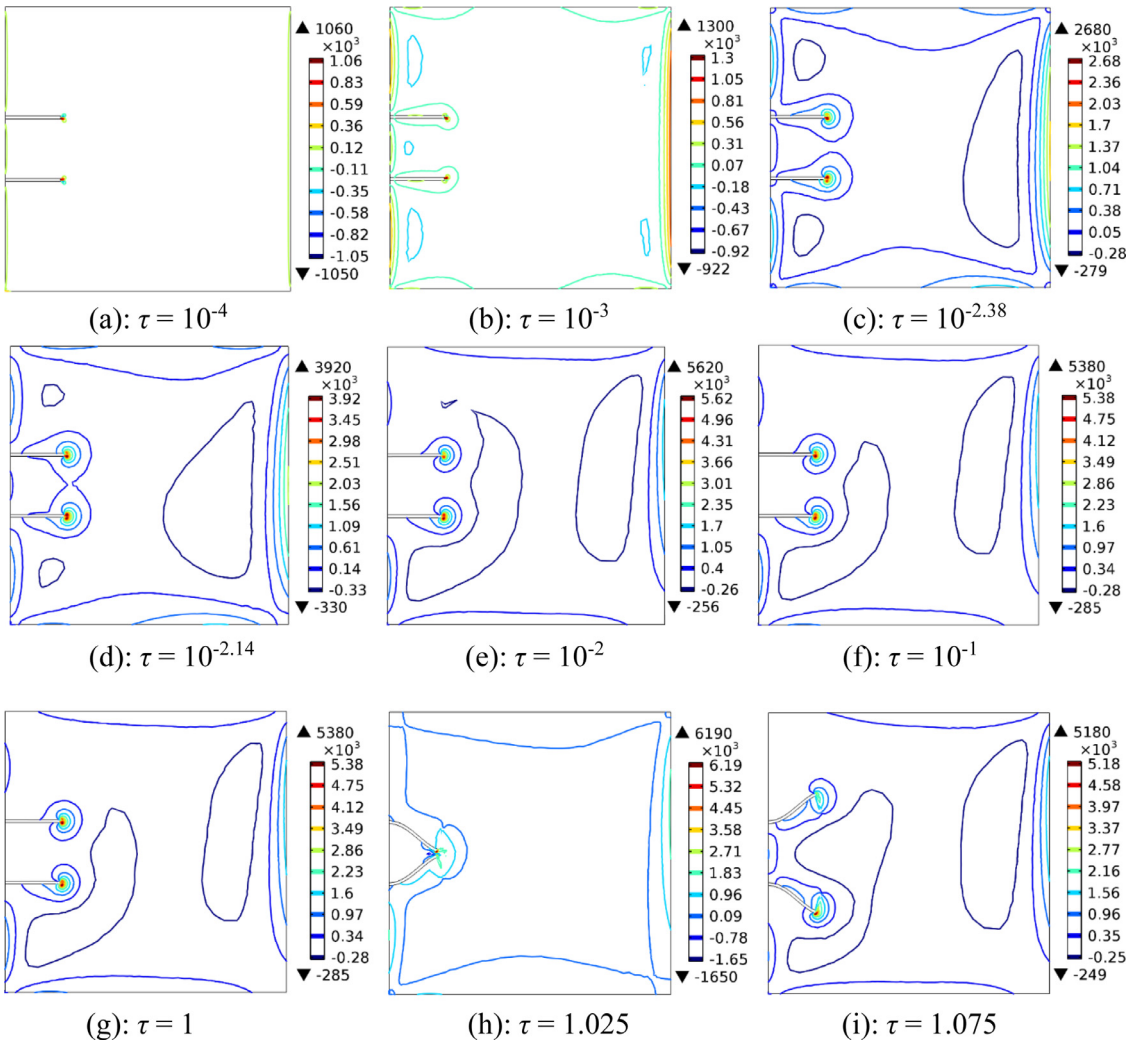

Fig. 10. Vorticity contours in the cavity over time.

number was high in the bottom areas. A slight increase in heat transfer along the lowest segment of the hot wall was due to the increased fluid velocity. There was a significant reduction in the temperature gradient between the fluid and warm wall, and the fluid along the hot wall contributed to the decreased local heat transfer. On the middle segment of the hot wall, the low velocity of the fluid adjacent to the heated fins led to a lower Nusselt number.

According to Fig. 12(a), (b), and (c), the local Nusselt numbers were more significant for the nanofluid compared with the pure fluid. Indeed, the nanoparticles in the base fluid enhanced the conductivity of the nanofluid. Figs. 12(a) and (b) show that the nanoparticles dispersed inside the base fluid did not significantly affect the local heat transfer rate on the lowest segment of the wall, but the effects of the dispersed nanoparticles on the local heat transfer rate on the middle of the wall were increasingly higher when the fins were rigid.

Furthermore, the rigidity and flexibility of the fins affected the local Nusselt number. The flexibility of the fins could either weaken or enhance the local heat transfer rate. The local heat transfer rate on the lowest segment of the hot wall was only slightly affected by the flexibility of the fins. However, the local heat transfer rates for the middle and highest parts of the wall were influenced dramatically by the oscillating fins. The oscillation of the fins improved the heat transfer rate through the middle part of the wall, but the reverse trend was found for the highest part of the hot wall.

Figs. 13(a) and (b) illustrate the effects of the frequency and oscillation amplitude, respectively, on the average Nusselt number in non-dimensional time steps from 1–2. According to Fig. 13(a), under a constant oscillation amplitude ($A = 0.1$) for the oscillating fins, increasing the oscillation frequency led to a decrease in the Nusselt number amplitude and an increase in the wavelength. Thus, the peak of the heat transfer for the nanofluid at a higher oscillation frequency, i.e., $\lambda = 0.5$, was reduced compared with the lower frequencies in the overall time step sequence. In addition, the oscillation amplitude

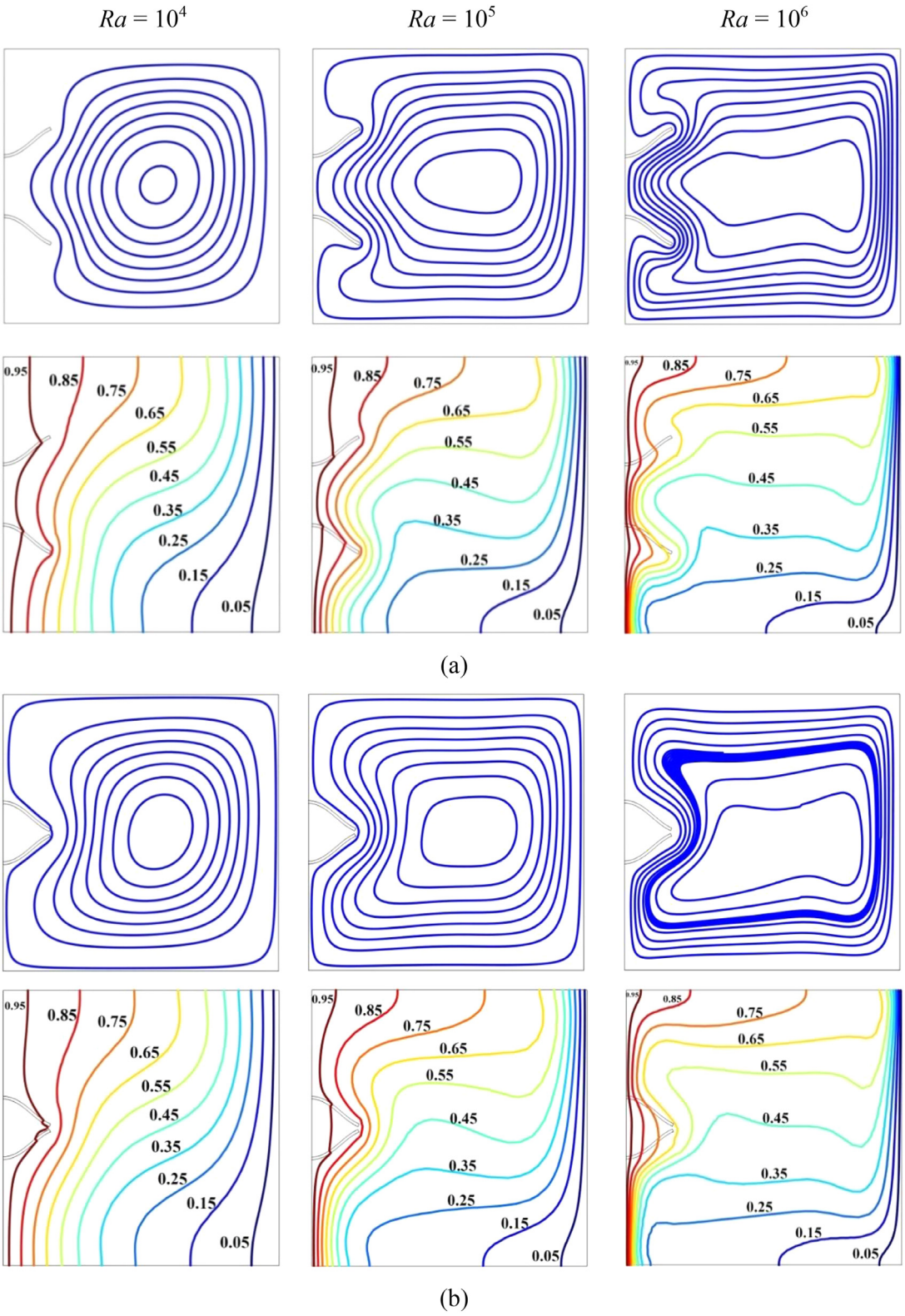

Fig. 11. Isotherms and streamlines under (a) opened fins and (b) closed fins conditions at different Rayleigh numbers.

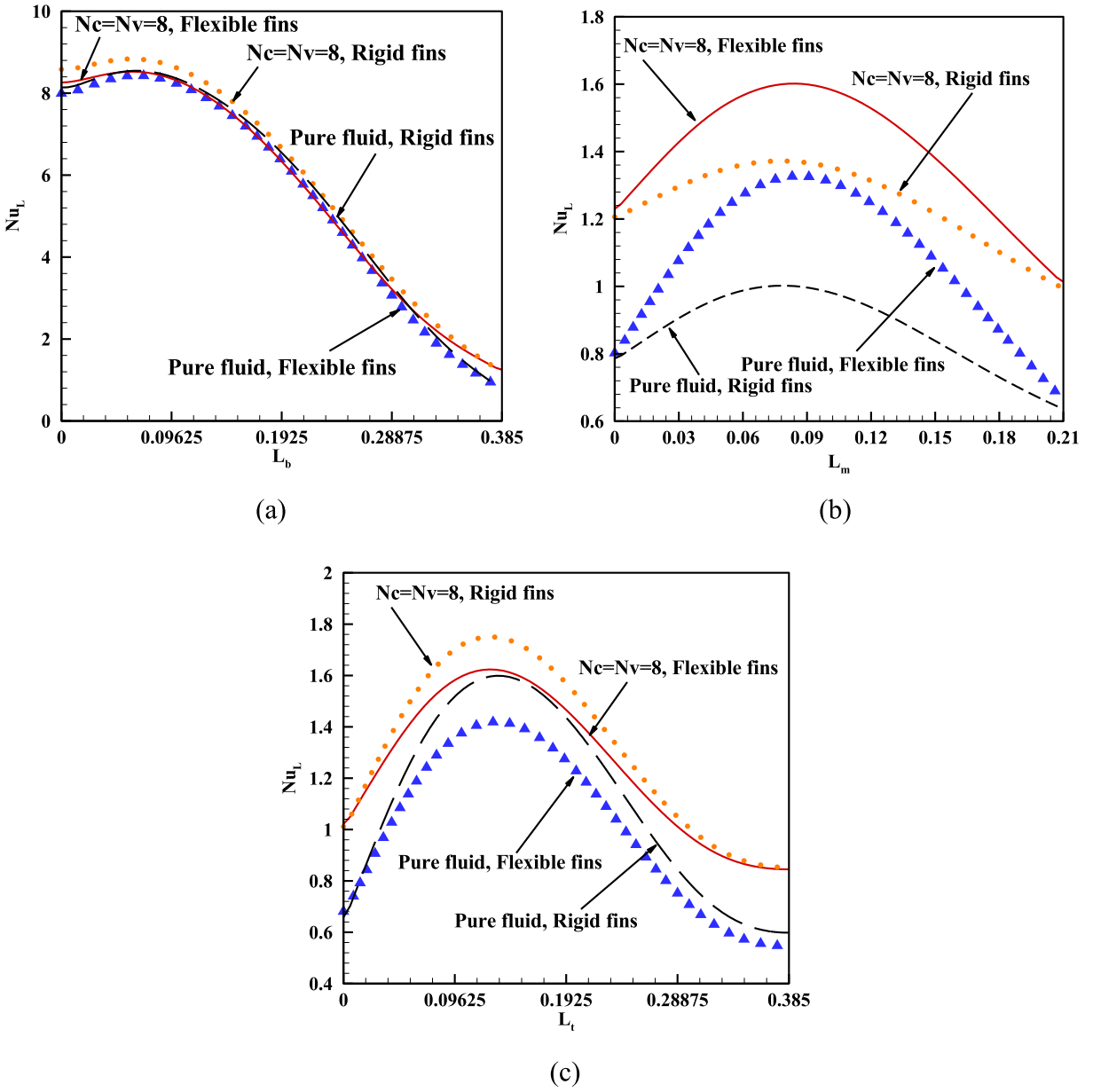

Fig. 12. Effects of conductivity and viscosity parameters (i.e., *Nc* and *Nv*) on the local Nusselt number on the: (a) hot wall below the fins, (b) hot wall between the two fins, and (c) top of the hot wall above the fins.

was lower at the average Nusselt number for the nanofluid at a higher frequency, i.e., $\lambda = 0.5$, than weak frequencies. The time-averaged Nusselt number decreased as the frequency increased.

Fig. 13(b) shows the effects of the oscillation amplitude for the flexible fins on the average Nusselt number at a constant frequency of $\lambda = 0.1$ in non-dimensional time steps from 1–2. Increasing the oscillation amplitude for the fins was directly related to increases in the average Nusselt number. Furthermore, according to the pattern obtained, increasing the oscillation amplitude by up to 10 times (from 0.01–0.1) led to increases in the time-averaged Nusselt number (4.639 to 4.76) in the overall time step sequence.

Fig. 14 shows the significant impacts of the ratio of the thermal conductivity of the flexible fins relative to the nanofluid, i.e., κ, on the average Nusselt number. At the primary times (10^{-8} to 10^{-4}), due to the intense thermal differences between the nanofluid and hot wall, the average Nusselt number was high at all thermal conductivity ratios. In fact, increasing κ led to greater heat transfer to the flow domain, thereby enhancing the driven buoyancy force. Moreover, increasing parameter κ at the primary times affected the average Nusselt number, where the heat transfer by the nanofluid decreased considerably

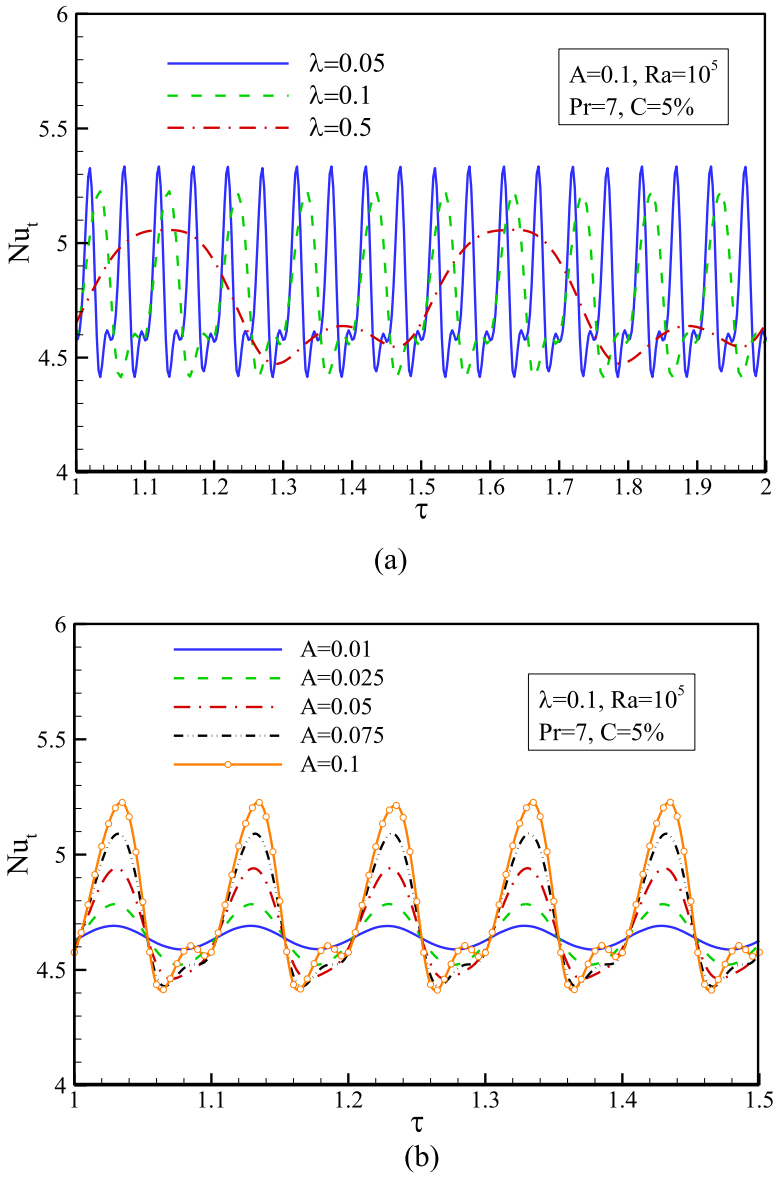

Fig. 13. Effects of (a) frequency λ and (b) amplitude A on the Nusselt number.

even at higher parameter κ values. Thus, although the effect of parameter κ was significant on the average Nusselt number during the primary times (10^{-8} to 10^{-3}), this trend was not observed after $\tau = 10^{-3}$. Subsequently ($\tau = 1$), the fins reached a quasi-steady state and started oscillating. As shown in Fig. 14(b), the variations in the Nusselt number from τ = 1– 1.5 exhibited an oscillating trend versus time. However, $\kappa = 1000$ obtained the minimal oscillation amplitude and $\kappa = 1$ yielded the maximum oscillation amplitude. Hence, $\kappa = 1000$ and $\kappa = 1$ provided the maximum and minimum heat transfer rates, respectively, because the higher conductivity ratio led to a higher rate of heat transfer.

Figs. 15(a) and (b) illustrate the effects of the thermal conductivity *Nc* and dynamic viscosity *Nv* parameters, respectively, on the heat transfer by the nanofluid. These parameters depend on the material, size, and form of the nanoparticles, as well as the properties of the base fluid and working temperature. Thus, each nanofluid has particular thermal conductivity and dynamic viscosity parameters. For instance, a water–alumina nanofluid containing spherical nanoparticles with a diameter of 40 nm at an ambient temperature of $T = 25$°C has values of $Nc = 23$ and $Nv = 2.88$. Figs. 15(a) and (b) show the plots obtained for different parameters with a nanoparticle volume fraction of 5% where: (a) $Nc = 8$ and $Nv = 4$, (b) $Nc = Nv = 8$, and (c) $Nc = 4$ and $Nv = 8$. According to the figure on the left in Fig. 15, the heat transfer by the four nanofluids was higher than that by the pure fluid at the primary times. The fluid flow became uniform after passing the transient section and all five plots approached each other until the fins started oscillating. According to the figure on the right in Fig. 15, the total

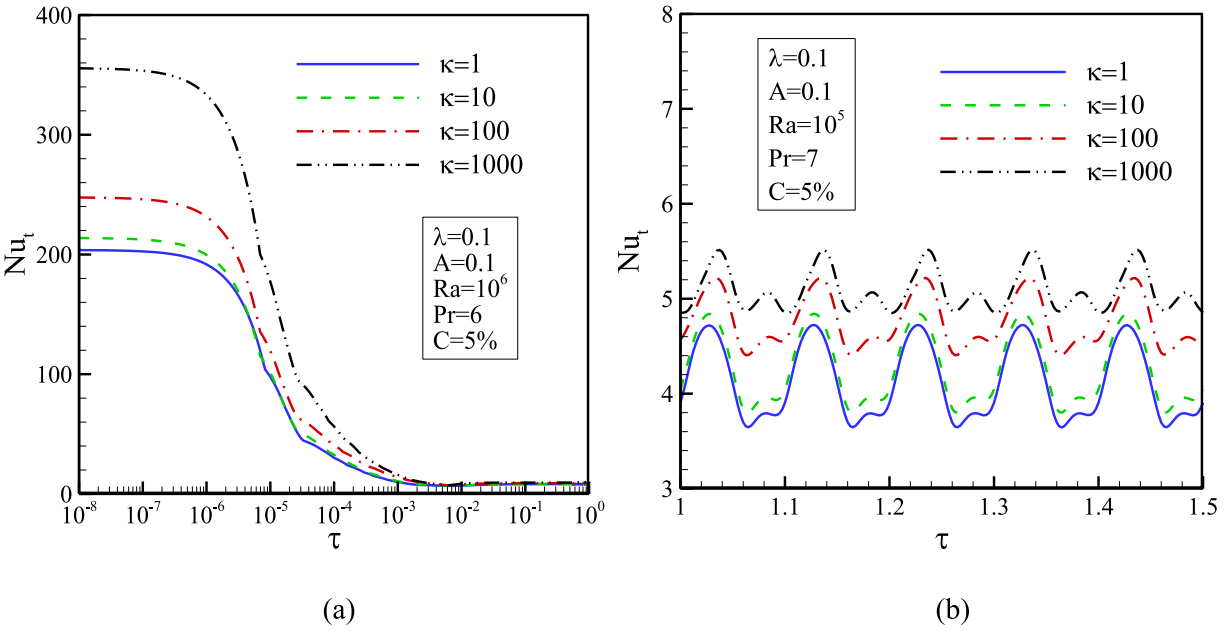

Fig. 14. Variations in the Nusselt number at different non-dimensional times at several parameter κ values.

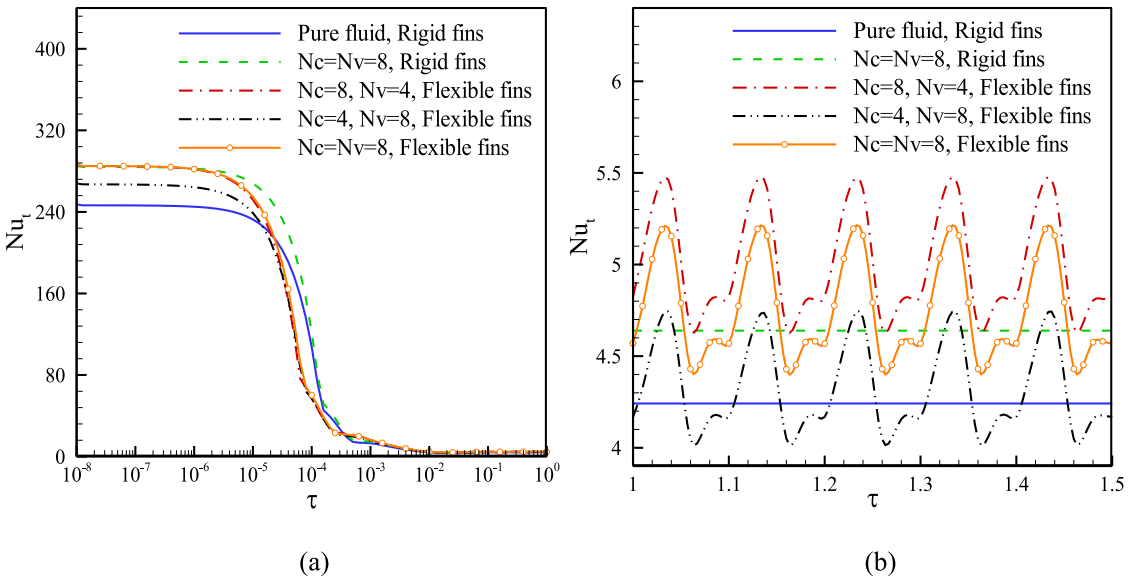

Fig. 15. Effects of conductivity and viscosity parameters (i.e., *Nc* and *Nv*) on the average Nusselt numbers using the default parameter values.

heat transfer rate increased and decreased as parameters *Nc* and *Nv* increased, respectively. In fact, increasing parameters *Nc* and *Nv* increased the thermal conductivity and viscosity resistance, respectively. Comparisons of the heat transfer rates for a specified nanofluid with rigid and flexible fins indicated that the heat transfer rate increased while the fins oscillated.

Figs. 16(a) and (b) show the effects of the nanoparticle volume fraction on the heat transfer rate. The figure on the left in Fig. 16 compares the average Nusselt numbers for the three volume fractions of 2%, 5%, and 8% with the pure fluid when using flexible and rigid fins. At the primary times when the fins did not oscillate, the effect of the nanoparticles inside the base fluid was significant, and increasing the volume fraction considerably enhanced the heat transfer. The higher range of the Nusselt number for larger nanofluid volume fractions decreased over time, and all the plots converged for the nanofluids and base fluid. According to the figure on the right in Fig. 16, dispersing the nanoparticles in the base fluid improved the heat transfer rate regardless of the flexibility of the fins. The local extrema of the average Nusselt number became more apparent as the nanoparticle volume fraction increased. Moreover, comparisons of the average Nusselt numbers obtained

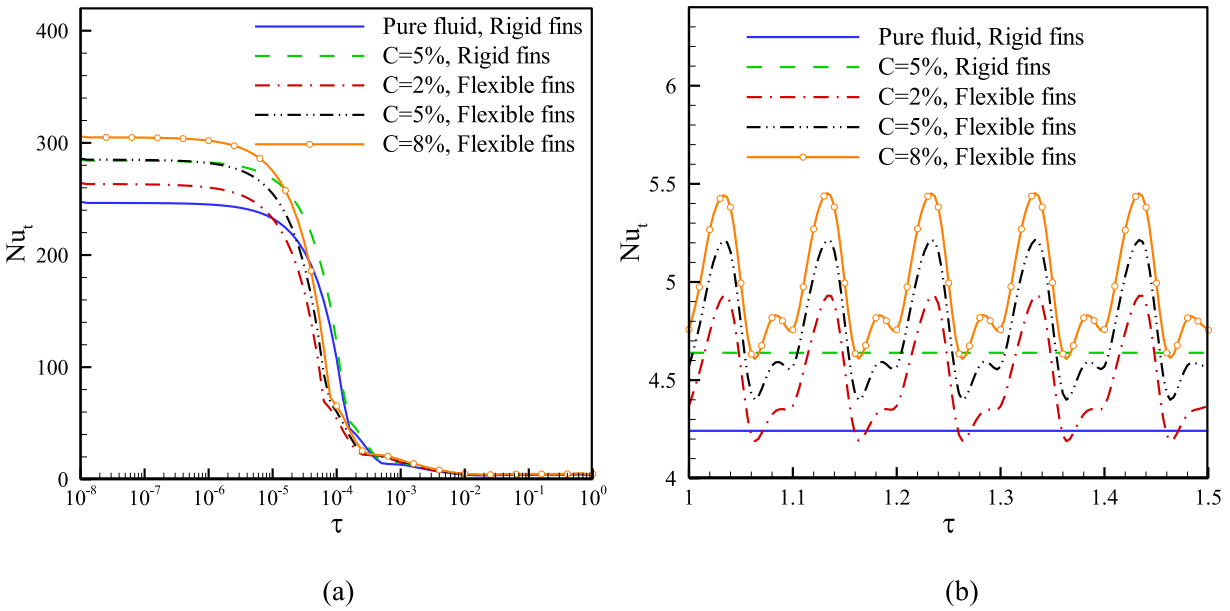

Fig. 16. Effects of the nanoparticle volume fraction of on the average Nusselt number using the default parameter values.

Table 4
Average Nusselt number based on five cycles for various values of κ.

κ	Nu_{avg} (Flexible fins)	Nu_{avg} (Rigid fins)
1	4.1208	3.9893
10	4.2590	4.1241
100	4.7564	4.6383
1000	5.0875	4.9762

for the flexible and rigid fins with the nanofluid at $C = 5\%$ clearly indicated that oscillation slightly improved the heat transfer rate. In fact, the increasing the fluid velocity near the fins while the fins oscillated increased the heat transfer rate.

Table 4 shows the time-averaged Nusselt numbers for different thermal conductivity ratio parameters, i.e., κ. The heat transfer rate increased as this parameter increased. When the thermal conductivity of the fins was low, the heat transfer by the nanofluid only occurred next to the vertical hot wall and the heat at the base of the fins made a minor contribution to the heat transfer. In this case, the fins only deflected the flow and they were not beneficial from a heat efficiency viewpoint. In addition, the effect of the flexibility of the fins on the increase in the heat transfer rate decreased as the thermal conductivity ratio increased.

5. Conclusion

This study investigated the heat transfer in a cavity filled with a nanofluid. Two types of solid and flexible fins were attached to the warm wall of the cavity, and the effects of fin oscillation on the heat transfer rate were determined. The fins started oscillating when the natural convection reached a steady state. The following conclusions can be made based on the results obtained by numerical investigation.

- The flexibility of the fins could either weaken or enhance the local heat transfer rate. The oscillation of the fins improved the rate heat transfer through the middle part. However, the local heat transfer was reduced at the highest part of the hot wall when the fins oscillated.
- Increasing the frequency of the oscillations decreased the Nusselt number amplitude and increased the wavelength. The time-averaged Nusselt number also decreased as the frequency increased.
- Increasing the oscillation amplitude for the fins led to increases in the average Nusselt number.
- The maximum and minimum average Nusselt numbers were obtained when $\kappa = 1000$ and 1, respectively. In addition, the average Nusselt number had the lowest oscillation amplitude when $\kappa = 1000$ and the maximum oscillation amplitude when $\kappa = 1$. Moreover, the impact of the flexibility of the fins on the average Nusselt number was higher at lower thermal conductivity ratios.
- The local Nusselt numbers were higher with the nanofluid compared with the pure fluid. The heat transfer rates increased and decreased as the thermal conductivity and viscosity parameters increased, respectively.

In the present study, the space between the fins and inclination angles of the fins were assumed to be fixed. The results showed that the presence of fins and their oscillation significantly affected the flow and heat transfer in the cavity. Hence, geometrical effects such as the fin inclination angle and the space between the fins may be investigated in future studies.

Supplementary material

Supplementary material associated with this article can be found, in the online version, at doi:10.1016/j.apm.2019.12.018.

References

[1] D.D. Ganji, S.H.H. Kachapi, Chapter 6 - Natural, mixed, and forced convection in nanofluid, in: D.D. Ganji, S.H.H. Kachapi (Eds.), Application of Nonlinear Systems in Nanomechanics and Nanofluids, William Andrew Publishing, Oxford, 2015, pp. 205–269.
[2] R. Iwatsu, J.M. Hyun, K. Kuwahara, Mixed convection in a driven cavity with a stable vertical temperature gradient, International Journal of Heat and Mass Transfer 36 (1993) 1601–1608.
[3] H.F. Oztop, I. Dagtekin, Mixed convection in two-sided lid-driven differentially heated square cavity, International Journal of Heat and Mass Transfer 47 (2004) 1761–1769.
[4] H. Lamarti, M. Mahdaoui, R. Bennacer, A. Chahboun, Numerical simulation of mixed convection heat transfer of fluid in a cavity driven by an oscillating lid using lattice Boltzmann method, International Journal of Heat and Mass Transfer 137 (2019) 615–629.
[5] T. Radhakrishnan, A. Verma, C. Balaji, S. Venkateshan, An experimental and numerical investigation of mixed convection from a heat generating element in a ventilated cavity, Experimental Thermal and Fluid Science 32 (2007) 502–520.
[6] S. Houat, Z.E. Bouayed, The lattice Boltzmann method for mixed convection in a cavity, Energy Procedia 139 (2017) 186–191.
[7] A.I. Alsabery, F. Selimefendigil, I. Hashim, A.J. Chamkha, M. Ghalambaz, Fluid-structure interaction analysis of entropy generation and mixed convection inside a cavity with flexible right wall and heated rotating cylinder, International Journal of Heat and Mass Transfer 140 (2019) 331–345.
[8] M. Probyn, B. Thornber, D. Drikakis, D. Youngs, R. Williams, An investigation into nonlinear growth rate of two-dimensional and three-dimensional single-mode Richtmyer–Meshkov Instability using an arbitrary-Lagrangian–Eulerian algorithm, Journal of Fluids Engineering 136 (2014) 091208.
[9] S.U.S. Choi, J. Eastman, Enhancing thermal conductivity of fluids with nanoparticles, Argonne National Lab., ILUnited States, 1995.
[10] A. Zeiny, H. Jin, L. Bai, G. Lin, D. Wen, A comparative study of direct absorption nanofluids for solar thermal applications, Solar Energy 161 (2018) 74–82.
[11] S. Vellaiyan, A. Subbiah, P. Chockalingam, Multi-response optimization to obtain better performance and emission level in a diesel engine fueled with water-biodiesel emulsion fuel and nanoadditive, Environmental Science and Pollution Research 26 (2019) 4833–4841.
[12] N. Yadav, A.K. Jaiswal, K.K. Dey, V.B. Yadav, G. Nath, A.K. Srivastava, R.R. Yadav, Trimetallic Au/Pt/Ag based nanofluid for enhanced antibacterial response, Materials Chemistry and Physics 218 (2018) 10–17.
[13] S. Mirmasoumi, A. Behzadmehr, Effect of nanoparticles mean diameter on mixed convection heat transfer of a nanofluid in a horizontal tube, International Journal of Heat and Fluid Flow 29 (2008) 557–566.
[14] S. Sarkar, S. Ganguly, G. Biswas, Mixed convective heat transfer of nanofluids past a circular cylinder in cross flow in unsteady regime, International Journal of Heat and Mass Transfer 55 (2012) 4783–4799.
[15] A. Aghanajafi, D. Toghraie, B. Mehmandoust, Numerical simulation of laminar forced convection of water-CuO nanofluid inside a triangular duct, Physica E: Low-Dimensional Systems and Nanostructures 85 (2017) 103–108.
[16] F. Selimefendigil, H.F. Öztop, Mixed convection of nanofluids in a three dimensional cavity with two adiabatic inner rotating cylinders, International Journal of Heat and Mass Transfer 117 (2018) 331–343.
[17] A.K. Kareem, S. Gao, Computational study of unsteady mixed convection heat transfer of nanofluids in a 3D closed lid-driven cavity, International Communications in Heat and Mass Transfer 82 (2017) 125–138.
[18] S. Kakaç, A. Pramuanjaroenkij, Review of convective heat transfer enhancement with nanofluids, International Journal of Heat and Mass Transfer 52 (2009) 3187–3196.
[19] S. Izadi, T. Armaghani, R. Ghasemiasl, A.J. Chamkha, M. Molana, A comprehensive review on mixed convection of nanofluids in various shapes of enclosures, Powder Technology 343 (2019) 880–907.
[20] H.K. Dawood, H.A. Mohammed, N.A. Che Sidik, K.M. Munisamy, M.A. Wahid, Forced, natural and mixed-convection heat transfer and fluid flow in annulus: A review, International Communications in Heat and Mass Transfer 62 (2015) 45–57.
[21] M. Elsebay, I. Elbadawy, M. Shedid, M. Fatouh, Numerical resizing study of Al_2O_3 and CuO nanofluids in the flat tubes of a radiator, Applied Mathematical Modelling 40 (2016) 6437–6450.
[22] O. Ghaffarpasand, Numerical study of MHD natural convection inside a sinusoidally heated lid-driven cavity filled with Fe3O4-water nanofluid in the presence of Joule heating, Applied Mathematical Modelling 40 (2016) 9165–9182.
[23] A. Raees, M. Raees-ul-Haq, H. Xu, Q. Sun, Three-dimensional stagnation flow of a nanofluid containing both nanoparticles and microorganisms on a moving surface with anisotropic slip, Applied Mathematical Modelling 40 (2016) 4136–4150.
[24] K. Deepak, M. Frank, D. Drikakis, N. Asproulis, Thermal properties of a water-copper nanofluid in a graphene channel, Journal of Computational and Theoretical Nanoscience 13 (2016) 79–83.
[25] M. Frank, D. Drikakis, Solid-like heat transfer in confined liquids, Microfluidics and Nanofluidics 21 (2017) 148.
[26] M. Frank, D. Drikakis, N. Asproulis, Thermal conductivity of nanofluid in nanochannels, Microfluidics and nanofluidics 19 (2015) 1011–1017.
[27] M. Frank, M. Kio, D. Drikakis, L. Könözsy, N. Asproulis, Mass and stiffness effects on thermal resistance at the solid–liquid interface of nanofluidic channels, Journal of Computational and Theoretical Nanoscience 15 (2018) 141–146.
[28] M. Papanikolaou, M. Frank, D. Drikakis, Nanoflow over a fractal surface, Physics of Fluids 28 (2016) 082001.
[29] K.M. Khanafer, A.M. Al-Amiri, I. Pop, Numerical simulation of unsteady mixed convection in a driven cavity using an externally excited sliding lid, European Journal of Mechanics-B/Fluids 26 (2007) 669–687.
[30] D. Kashyap, A.K. Dass, Effect of boundary conditions on heat transfer and entropy generation during two-phase mixed convection hybrid Al_2O_3-Cu/water nanofluid flow in a cavity, International Journal of Mechanical Sciences 157–158 (2019) 45–59.
[31] M.A. Ismael, H.F. Jasim, Role of the fluid-structure interaction in mixed convection in a vented cavity, International Journal of Mechanical Sciences 135 (2018) 190–202.
[32] A. Ben-Nakhi, A.J. Chamkha, Conjugate natural convection in a square enclosure with inclined thin fin of arbitrary length, International Journal of Thermal Sciences 46 (2007) 467–478.
[33] N.B. Cheikh, A.J. Chamkha, B.B. Beya, Effect of inclination on heat transfer and fluid flow in a finned enclosure filled with a dielectric liquid, Numerical Heat Transfer, Part A: Applications 56 (2009) 286–300.
[34] A. Ben-Nakhi, A. Chamkha, Effect of length and inclination of a thin fin on natural convection in a square enclosure, Numerical Heat Transfer 50 (4) (2006) 381–399.
[35] A. Ben-Nakhi, A.J. Chamkha, Conjugate natural convection around a finned pipe in a square enclosure with internal heat generation, International Journal of Heat and Mass Transfer 50 (2007) 2260–2271.
[36] W. Zhao, A.K. Mozumder, P.K. Das, Mixed convection of CuO-water nanofluid in a square enclosure with an intruded rectangular fin, in: AIP Conference Proceedings, 2018.

[37] M.H. Yang, R.H. Yeh, Optimization of fin arrays in an inclined channel for mixed convection, Applied Thermal Engineering 148 (2019) 963–976.
[38] R.Z. Homod, F.A. Abood, S.M. Shrama, A.K. Alshara, Empirical correlations for mixed convection heat transfer through a fin array based on various orientations, International Journal of Thermal Sciences 137 (2019) 627–639.
[39] P.T. Barton, D. Drikakis, E. Romenski, An Eulerian finite-volume scheme for large elastoplastic deformations in solids, International Journal for Numerical Methods in Engineering 81 (2010) 453–484.
[40] R. Rannacher, Finite element methods for the incompressible Navier-Stokes equations, Fundamental directions in mathematical fluid mechanics, Fundamental directions in mathematical fluid mechanics, Birkhäuser, Basel, 2000, pp. 191–293.
[41] V. Girault, P.-A. Raviart, Finite element methods for Navier-Stokes equations: theory and algorithms (Vol. 5), Springer Science & Business Media, 2012.
[42] F. Thomasset, Implementation of finite element methods for Navier-Stokes equations, Springer Science & Business Media, 2012.
[43] J. Ludwig, S. Mortimor, PHOENICS-VR reference guide, CHAM, London, 2010.
[44] J.-F. Sigrist, Fluid-structure interaction: an introduction to finite element coupling, John Wiley & Sons, 2015.
[45] P.B. Ryzhakov, E. Oñate, A finite element model for fluid–structure interaction problems involving closed membranes, internal and external fluids, Computer Methods in Applied Mechanics and Engineering 326 (2017) 422–445.
[46] E. Oñate, J. Garcıa, A finite element method for fluid–structure interaction with surface waves using a finite calculus formulation, Computer Methods in Applied Mechanics and Engineering 191 (2001) 635–660.
[47] M. Ghalambaz, E. Jamesahar, M.A. Ismael, A.J. Chamkha, Fluid-structure interaction study of natural convection heat transfer over a flexible oscillating fin in a square cavity, International Journal of Thermal Sciences 111 (2017) 256–273.
[48] F. Selimefendigil, H.F. Oztop, A.J. Chamkha, MHD mixed convection in a nanofluid filled vertical lid-driven cavity having a flexible fin attached to its upper wall, Journal of Thermal Analysis and Calorimetry 135 (2019) 325–340.
[49] A. Raisi, I. Arvin, A numerical study of the effect of fluid-structure interaction on transient natural convection in an air-filled square cavity, International Journal of Thermal Sciences 128 (2018) 1–14.
[50] S.M.H. Zadeh, S. Mehryan, E. Izadpanahi, M. Ghalambaz, Impacts of the flexibility of a thin heater plate on the natural convection heat transfer, International Journal of Thermal Sciences 145 (2019) 106001.
[51] A. Alsabery, M. Sheremet, M. Ghalambaz, A. Chamkha, I. Hashim, Fluid-structure interaction in natural convection heat transfer in an oblique cavity with a flexible oscillating fin and partial heating, Applied Thermal Engineering 145 (2018) 80–97.
[52] S.A.M. Mehryan, A.J. Chamkha, M.A. Ismael, M. Ghalambaz, Fluid–structure interaction analysis of free convection in an inclined square cavity partitioned by a flexible impermeable membrane with sinusoidal temperature heating, Meccanica 52 (2017) 2685–2703.
[53] E. Jamesahar, M. Ghalambaz, A.J. Chamkha, Fluid–solid interaction in natural convection heat transfer in a square cavity with a perfectly thermal-conductive flexible diagonal partition, International Journal of Heat and Mass Transfer 100 (2016) 303–319.
[54] A. Zaraki, M. Ghalambaz, A.J. Chamkha, M. Ghalambaz, D. De Rossi, Theoretical analysis of natural convection boundary layer heat and mass transfer of nanofluids: Effects of size, shape and type of nanoparticles, type of base fluid and working temperature, Advanced Powder Technology 26 (2015) 935–946.
[55] O.C. Zienkiewicz, R. Taylor, P. Nithiarasu (Eds.), The Finite Element Method for Fluid Dynamics, (Seventh Edition), Butterworth-Heinemann, 2014, p. iii. https://www.elsevier.com/books/the-finite-element-method-for-fluid-dynamics/zienkiewicz/978-1-85617-635-4.
[56] U. Küttler, W. Wall, Fixed-point fluid-structure interaction solvers with dynamic relaxation, Computational mechanics 43 (1) (2008) 61–72.
[57] K. Kahveci, Buoyancy driven heat transfer of nanofluids in a tilted enclosure, Journal of Heat Transfer 132 (2010) 062501.